Proceedings of the 3rd Croatian Conference on Earthquake Engineering - 3CroCEE
19–22 March 2025, Split, Croatia

DOI: https://doi.org/10.5592/CO/3CroCEE.2025.24

NUMERICAL VALIDATION OF MASONRY WALL EXPERIMENTS USING THE APPLIED ELEMENT METHOD

Sergey Churilov [(1)]

[(1)] *Professor, Ss. Cyril and Methodius University in Skopje, Faculty of Civil Engineering Skopje, curilov@gf.ukim.edu.mk*

Abstract

This paper presents an investigation of unreinforced masonry (URM) walls under cyclic in-plane loading using the Applied Element Method (AEM). Due to their historical nature, masonry structures are highly relevant in modern construction; however, they normally pose certain challenges with regards to structural analysis because of their composite nature and nonlinear behaviour. While experimental investigations provide critical information about masonry behaviour, numerical modelling offers an efficient way to extend the understanding of structural performance under various loading conditions. The study combines experimental validation with numerical modelling to evaluate the seismic performance of masonry structures. Two full-scale URM walls with varying vertical pre-compression levels tested experimentally were selected for the validation. The walls exhibited shear-dominated failure mechanisms with diagonal cracking patterns. A simplified micro-modelling approach was implemented in AEM, incorporating nonlinear material behaviour and contact mechanisms. The numerical models accurately captured the experimental force-displacement relationships, with deviations in lateral strength predictions ranging from 2% to 10%. The simulations successfully reproduced the observed failure mechanisms, including crack initiation and propagation patterns. Initial stiffness was slightly overestimated, while displacement at peak lateral strength showed reasonable agreement with experimental results. The study demonstrates AEM's capability to model complex masonry behaviour, while the findings validate AEM as a reliable tool for seismic assessment of masonry structures, with important implications for both historic building conservation and modern masonry design.

Keywords: unreinforced masonry, applied element method (AEM), in-plane cyclic behaviour, seismic performance, numerical modelling, experimental validation.

1. Introduction

Masonry structures represent one of humanity's oldest construction forms, yet their structural analysis remains challenging due to their composite nature and material heterogeneity [1]. The complex dynamic behaviour of unreinforced masonry (URM) structures, characterized by heterogeneous composition and directionally dependent properties, presents significant challenges for seismic assessment [2]. Traditional analytical methods often fail to capture the intricate failure mechanisms and load-distribution patterns observed in real structures [3].

Recent advances in computational mechanics have enabled more sophisticated approaches to masonry analysis. While finite element methods (FEM) have emerged as powerful tools [4], the reliability of numerical models heavily depends on proper validation against experimental data. As noted by Theodossopoulos and Sinha [5], validation processes serve to verify computational results and refine understanding of masonry behaviour under various loading conditions.

The Applied Element Method (AEM), initially developed by Meguro and Tagel-Din [6], represents a significant advancement in structural analysis techniques. Unlike traditional FEM, AEM discretizes structures into small rigid elements connected by normal and shear springs [7, 8], allowing simulation from initial loading through complete collapse [9]. In AEM, masonry structures are modelled using brick springs (connecting elements within bricks) and brick-mortar interface springs (connecting elements between different bricks), effectively capturing the composite nature of masonry [8–10]. AEM offers several advantages for masonry analysis. As demonstrated by Eraky et al. [11], it can analyse

Proceedings of the 3rd Croatian Conference on Earthquake Engineering - 3CroCEE
19–22 March 2025, Split, Croatia

DOI: https://doi.org/10.5592/CO/3CroCEE.2025.24

structural behaviour without requiring prior assumptions about crack locations or propagation directions. The method excels in representing complex mechanical behaviours, particularly rigid body motion and element collision scenarios, while typically requiring less modelling time compared to FEM approaches [11]. One key advantage over FEM is that no transition elements are needed, as elements are connected at faces, allowing partial connectivity [12]. The reliability of AEM has been validated through several studies comparing numerical predictions with experimental observations. These comparisons have shown remarkable concordance, particularly in the prediction of failure patterns and load-displacement relationships. Recent studies have validated AEM's effectiveness for masonry analysis both in-plane and out-of-plane and progressive collapse scenarios, with predictions achieving accuracy within 20% of experimental results [13–16]. While highly effective, the method requires careful material parameter calibration and faces computational intensity challenges with complex models [13, 14, 17, 18].

Despite these advances, several critical research gaps remain in the application of AEM to masonry structures, particularly regarding historic construction and dynamic behaviour. The interaction between in-plane and out-of-plane forces remains underexplored, especially in the context of complex wall assemblies typical in historic buildings [13]. While static and quasi-static analyses are well-documented, there is limited research on dynamic response simulation [7], creating a significant knowledge gap in understanding seismic behaviour. Current methods often prove too complex and computationally intensive for practical implementation in heritage conservation projects [8]. Although AEM has been successfully applied to simple URM structures, studies on complex geometries and irregular layouts characteristic of historic construction are scarce [14]. Current AEM models often use simplified material properties for masonry, neglecting variability due to aging and environmental factors [13]. Perhaps most significantly, while some studies have validated AEM results against experimental data, there is a notable scarcity of comparisons with full-scale URM building tests under dynamic loading up to collapse [13, 14]. This gap is particularly relevant for heritage structures where understanding complete collapse mechanisms is essential for seismic risk assessment.

While significant progress has been made in understanding the in-plane behaviour of masonry, the integration of experimental and numerical methods must continue to address the complexities of real-world applications, particularly in seismic-prone areas. This paper presents a comprehensive study of URM walls using AEM, incorporating experimental validation through comparison with shear behaviour tests. The research aims to establish reliable modelling strategies for predicting the seismic response of masonry structures while addressing current challenges in numerical simulation methods.

2. Experimental Program

The experimental investigation focused on evaluating the in-plane cyclic behaviour of unreinforced masonry walls under seismic loading conditions [19, 20]. Four unreinforced masonry wall (URM) specimens were constructed using solid clay bricks and lime mortar to represent typical historical masonry construction, out of which two were selected in this study. Both URM walls were constructed using solid clay bricks (250×120×65 mm^3) and traditional lime mortar mix (1:3 lime:sand ratio). Material properties were experimentally determined through standardized testing procedures as shown in Table 1.

Masonry compressive strength tests on three wall specimens (520×320×125 mm^3) yielded a characteristic mean strength of $f_k = 3.0$ N/mm^2 and elastic modulus of $E = 2874.8$ N/mm^2 Shear strength characterization using nine masonry triplets under varying pre-compression stress levels (0.2, 0.6 and 1.0 N/mm^2) revealed a friction coefficient $\mu = 0.66$ (friction angle $\theta = 33.4°$). These material properties provided essential input parameters for subsequent numerical modelling and analysis of the masonry wall behaviour under various loading conditions. The relatively low strength values obtained are typical for historical masonry construction using lime mortar [21–23].

The test matrix comprised identical wall geometries (squat walls) under two vertical pre-compression levels of 0.5 N/mm^2 and 1.0 N/mm^2 (URM1, URM3), see Table 2.

DOI: https://doi.org/10.5592/CO/3CroCEE.2025.24

Table 1. Experimental material properties for bricks and mortar [19, 20]

Property	Brick	Mortar
Density, γ [kg/m^3]	1922.6	1384.7
Compressive strength, f_k [N/mm^2]	10.8	0.6
Tensile flexural strength, $f_{t,fl}$ [N/mm^2]	2.7	0.1

Table 2. Test specimen configuration and vertical compression stresses [20]

Walls	Length, L [mm]	Height, H [mm]	Slenderness ratio (H/L)	Vertical stress, σ_0 [N/mm^2]	σ_0/f_k ratio
URM1	2520	1820	0.72	1.0	0.33
URM3	2520	1820	0.72	0.5	0.17

The specimens were constructed on 250x400 mm^2 pre-casted RC foundation beams anchored to the rigid laboratory floor, with a pre-casted 250x250 mm^2 RC top beams incorporating steel roller bearings and elastomeric bearings to enable horizontal movement while maintaining vertical load distribution. Concrete with compressive strength of $f_c = 30$ N/mm^2, reinforced with 3Ø12 mm longitudinal rebars ($f_y = 400$ N/mm^2) and rectangular stirrups Ø8/100/200 mm were used [19].

The experimental investigation was conducted using a purpose-built steel testing frame equipped with both vertical and horizontal hydraulic actuators. Vertical actuators maintained constant axial loads throughout testing, while horizontal actuators imposed cyclic lateral displacements. The test setup incorporated a monitoring system consisting of strategically placed load cells (LC1-LC4) and displacement transducers (DT1-DT8), Figure 1a. Load cells monitored both vertical and horizontal forces, while displacement transducers tracked in-plane and out-of-plane deformations at critical locations along the wall height, Figure 1b.

The testing protocol followed a systematic approach, beginning with the application of vertical precompression loads. These loads were gradually applied and maintained constant throughout the test duration. Subsequently, quasi-static cyclic lateral loading was introduced following a predetermined displacement history as illustrated in Figure 1c.

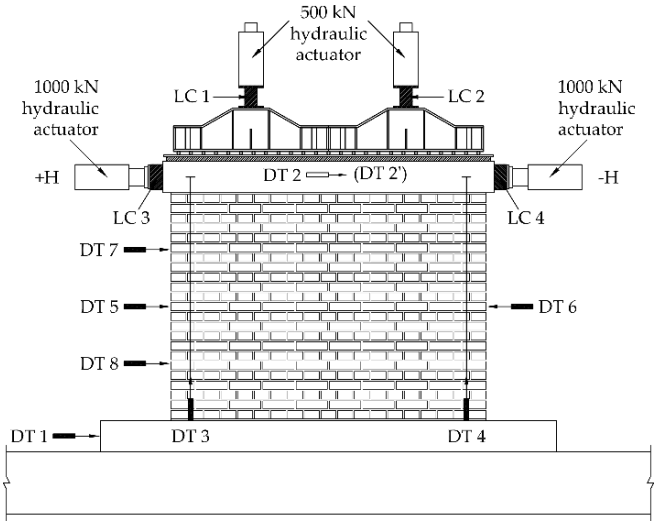

a) Schematics of the key components of the test setup and measuring points locations

b) DT2 sensor on the top RC beam

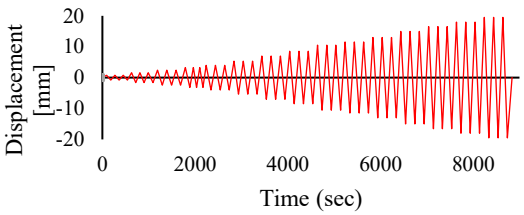

c) Horizontal displacement protocol

Figure 1. Experimental test setup [19, 20]

DOI: https://doi.org/10.5592/CO/3CroCEE.2025.24

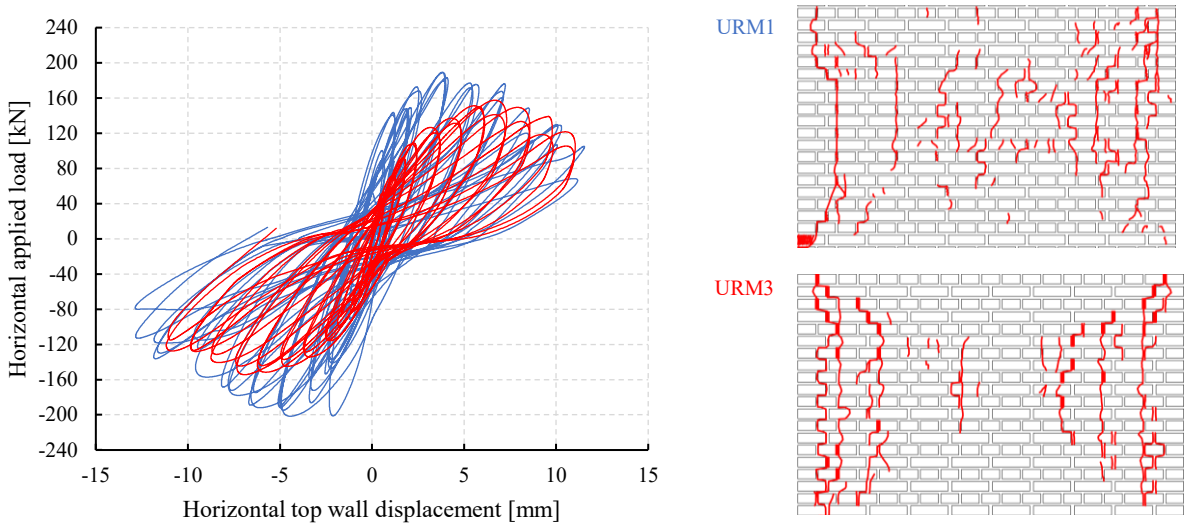

Figure 2. Experimental force-displacement hysteresis diagrams and failure of URM walls

Each displacement amplitude was repeated for three complete cycles to assess strength and stiffness degradation. Loading rates were carefully controlled between 0.2 and 0.5 kN/s to minimize dynamic effects while ensuring test efficiency. Throughout testing, the vertical actuators were manually controlled to prevent in-plane rotation of the top RC beam, maintaining the desired "double-fixed" boundary conditions. The experimental investigation revealed consistent behaviour patterns across all specimens, characterized predominantly by shear-dominated failure mechanisms.

Both URM walls (URM1 and URM3) primarily developed vertically oriented cracks passing through bricks or along head joints, Figure 2. The force-displacement relationships demonstrated almost symmetrical behaviour in both positive and negative loading directions. Initial response remained elastic until the formation of first cracks, occurring at drift ratios between 0.03% and 0.04%. The influence of precompression levels emerged as a significant factor affecting overall performance. URM1 subjected to higher vertical stress (1.0 N/mm^2) demonstrated increased lateral load capacity compared to its counterpart under lower precompression (0.5 N/mm^2).This behaviour aligns with previous research [24–28] and can be attributed to the higher principal tensile stresses required for wall failure. This enhancement in lateral strength was accompanied by improved energy dissipation capabilities, particularly evident in the post-peak response region. The force-displacement relationships exhibited peak lateral forces typically occurring at drift ratios of 0.29% and 0.46%, and drift ratios of 0.67% and 0.72% at the ultimate resistance levels for walls URM1 and URM3, respectively [19]. The precompression level had minimal influence on ultimate displacements, with URM3 actually achieving higher ultimate displacement than URM1. Stiffness degradation followed a consistent pattern across both walls, characterized by a power function relationship between normalized stiffness and displacement ductility. The equivalent viscous damping coefficient, calculated from hysteretic energy dissipation, averaged 12.6% at ultimate displacement levels for both walls, indicating significant energy dissipation capacity despite the brittle nature of the masonry material [20].

3. Numerical Modelling

3.1. Modelling strategy and assumptions

The Applied Element Method (AEM) offers a novel approach to structural analysis, especially for modelling collapse scenarios. The method differs fundamentally from traditional FE methods by representing structures through small, discrete elements interconnected by distributed normal and shear springs along their faces [6]. These spring sets effectively capture the complete mechanical behaviour: stresses, strains, and deformations of the corresponding material volume, as illustrated in Figures Figure 3-Figure 5.

DOI: https://doi.org/10.5592/CO/3CroCEE.2025.24

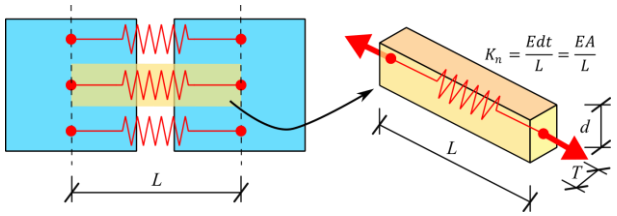

Figure 3. Stiffness of normal springs [29]

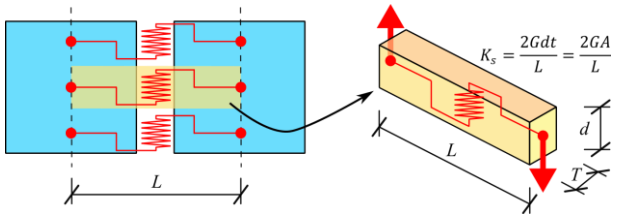

Figure 4. Stiffness of shear springs [29]

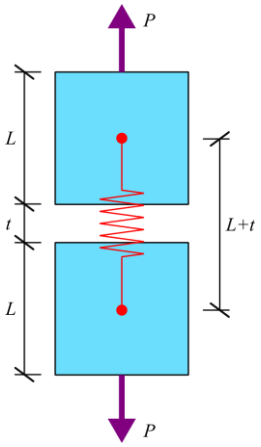

Figure 5. Modelling mortar thickness by averaging the properties for brick and mortar [29]

AEM's distinctive capability lies in its comprehensive simulation of structural response across all loading phases, from initial elastic behaviour through progressive damage and ultimate collapse [29]. Unlike traditional FEM approaches, AEM effectively handles discontinuous behaviour through automatic element separation and collision detection when spring elements exceed their ultimate strain limits. The stiffnesses of normal K_n and shear K_s springs are calculated as shown in (1).

$$K_n = \frac{EdT}{L} = \frac{EA}{L}; \qquad K_s = \frac{2GdT}{L} = \frac{2GA}{L} \tag{1}$$

where, E is tangent stiffness of the normal stress-normal strain curve, G is tangent stiffness of the shear stress-shear strain curve, d is distance between springs, T is thickness of the element, $A = dT$ is cross sectional area of the volume represented by the spring and L is distance between the centers of gravity of the connected elements [29].

The general formulation of AEM applied to masonry structures is discussed in detail in e.g. [6, 8, 29]. AEM offers three approaches for modelling masonry structures: detailed micro-modelling (units and mortar as rigid elements with spring interfaces), simplified micro-modelling (expanded units as rigid elements with lumped mortar behaviour in springs), and macro-modelling (homogeneous continuum approach) [30]. A simplified micro-modelling strategy approach was implemented in this study, building on established methodologies from multiple studies [7, 8, 13, 16, 17, 31, 32].

The simplified micro-modelling approach, implemented through the Extreme Loading for Structures (ELS) software, provides an optimal balance between computational efficiency and accuracy. In this approach, bricks are modelled in staggered configuration with zero-thickness springs representing mortar joints. In AEM the mass is concentrated in the rigid elements. Each brick can be further subdivided into smaller elements to allow for crack development within the brick itself. The composite brick-mortar behaviour is handled through equivalent springs with modified properties, considering brick and mortar as springs in series. As shown in Figure 5, the AEM accounts for the actual geometry of brick (length L) and mortar joint (thickness t) by using equivalent springs with modified (averaged) properties. The effective stiffness of these springs is derived by considering the brick and mortar as springs in series, leading to the formulation shown in (2):

$$K = \frac{E^* A}{L + t}; \qquad E^* = \frac{E_b E_m}{E_b t + E_m L} \times (L + t) \tag{2}$$

where, K is effective stiffness of the springs, E^* is the equivalent Young's modulus of elasticity for the spring, E_b and E_m are Young's modulus of elasticity for bricks and mortar, L is brick element size and t is mortar thickness.

DOI: https://doi.org/10.5592/CO/3CroCEE.2025.24

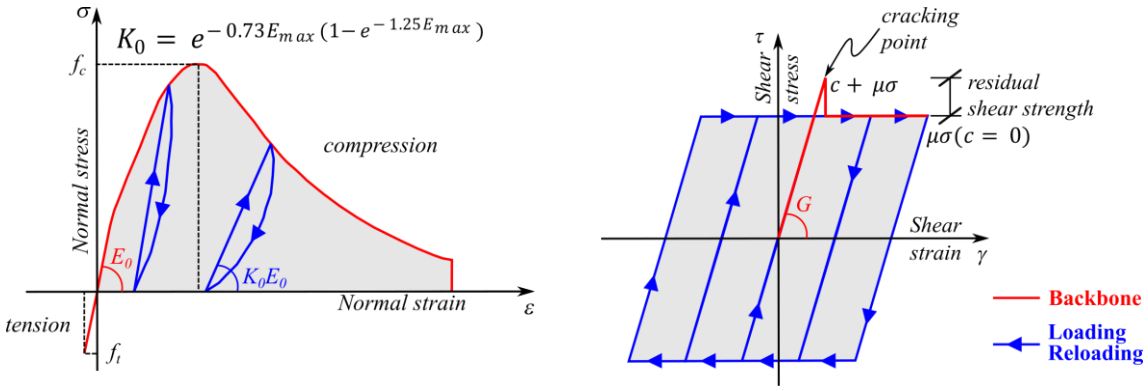

a) Normal springs b) Shear springs

Figure 6 Constitutive models for concrete and masonry [29]

The model's primary source of energy dissipation comes from hysteretic damping, which occurs during crack opening/closure and progressive damage evolution. This simplified damping approach has proven effective across numerous AEM applications, successfully analysing collapse mechanisms in both continuous and discrete blocky systems [15, 33].

The masonry nonlinear behaviour was modelled using the Concrete Maekawa model [34, 35], featuring a pseudo-parabolic compression envelope with tension cut-off and an elastic-plastic fracture model for cyclic loading, developed by El-Kashif and Maekawa [36] and shown in Figure 6. The model incorporates an elastic-plastic fracture response for compression, accounting for cyclic damage accumulation, while tensile behaviour follows a simplified linear failure envelope (brittle constitutive law without normal stiffness degradation) with a defined tensile strength limit (f_t) at zero shear stress.

The compression model incorporates three key parameters: initial Young's modulus (E_0), compressive plastic strain (ε_p) and a fracture parameter (K_0) governing stiffness and strength degradation. The fracture parameter is dynamically calculated using an exponential function of the maximum equivalent strain (E_{max}), as shown in Figure 6a and detailed in [33, 35]. In the shear response, the cohesion (c) reduces to zero once the maximum shear strength is reached (Figure 6b). The model incorporates Mohr-Coulomb yield criteria for shear behaviour without including shear stiffness degradation (Figure 6b). While the model effectively captures material capacity, hysteretic response, and deformation characteristics, it conservatively neglects residual shear strength under tensile conditions. The model's dynamic behaviour was handled through a sophisticated contact mechanism. Matrix springs are eliminated upon exceeding the separation strain threshold (default resultant of 0.1), while new contact springs form during re-contact, effectively simulating the interaction between distinct rigid bodies [29].

3.2. AEM model development for simulation of the in-plane cyclic tests

A simplified micro-modelling approach of a 3-D computational models of URM walls was applied using the AEM analysis implemented through ELS software [29], Figure 7. The masonry walls were modelled using their actual geometry, with clay bricks 255×125×70 mm^3 adjusted to accommodate mortar joint thicknesses of 10 mm arranged in an English-bond pattern. Individual bricks were represented as 3-D solid elements (rigid bodies) with eight nodes (3x8 DOF). Mortar joints were simulated through a grid of 25 nonlinear springs (5×5 pattern) at contact surfaces between bricks, following previously validated approaches [6–8], simulating the mechanical properties of bed and head joints. Mesh convergence analysis comparing full-sized and half-sized brick elements was performed to validate the block size selection. Joint behaviour incorporated Mohr-Coulomb failure criteria with complete post-failure cohesion degradation to zero for shear strength (Figure 6b), while tension followed a linear relationship with no post-peak response (Figure 6a). Material characterization integrated both experimental data [19, 20] and literature-derived parameters [7, 8, 10, 13, 30]. The calibration process involved iterative refinement of "preliminary" models, initially parameterized using experimental properties, to achieve optimal correlation with observed behaviour, as shown in Table 3.

DOI: https://doi.org/10.5592/CO/3CroCEE.2025.24

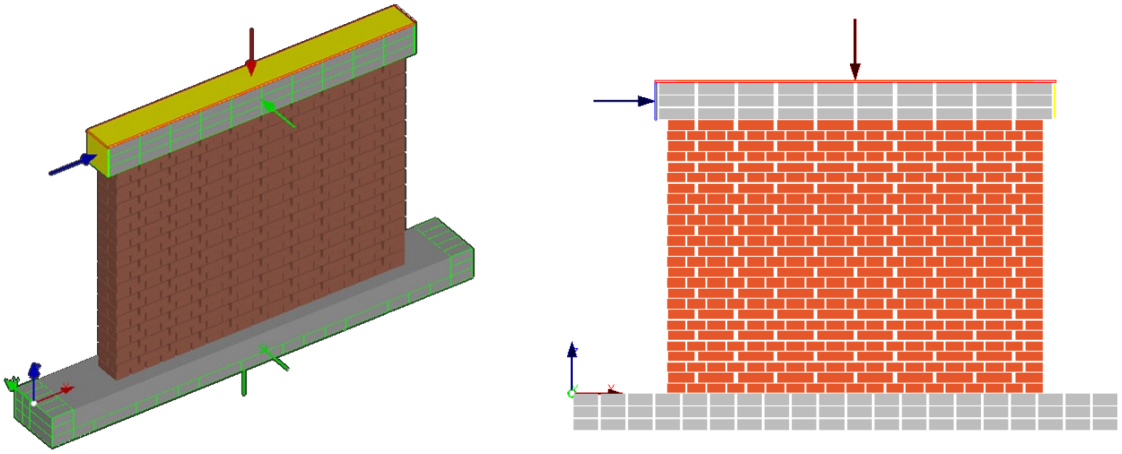

Figure 7 Developed AEM model (bricks and RC beams are shown as shrank)

Models were systematically calibrated against experimental data, resulting in so called "calibrated" models. In cases of limited experimental data, the Young's modulus (E) for the bricks can be estimated as $(200-1000)f_c$, where f_c is compressive strength, while the Poisson's ratio (ν) typically ranges 0.15-0.25 for masonry materials [30]. Direct tensile characterization remains challenging due to testing complexities.

The tensile strength (f_t) typically ranges $(0.03-0.1)f_c$, or can be determined by $f_t = 2.12\ln(1+0.075f_c)$ [30]. For the preliminary model, the Young's modulus of the bricks was estimated as $1{,}000f_c$, and the shear modulus (G) was calculated utilizing the equation $G = E/(2(1+\nu))$, with an assumed Poisson's ratio (ν) of 0.25. In situations where detailed experimental data is unavailable, the coefficient of friction (μ) can be approximated as 0.75 and in this study, it was varied in a range of 0.6-0.8. Furthermore, as established by Lourenço [37], the cohesion (c) can be estimated through its relationship with the tensile bond strength (f_t), expressed as $c = 1.4f_t$. The nonlinear material response was described through fracture energies. The recommended fracture energy in compression (G_c) was calculated with $G_c = 32/(10+f\_c)$ and the fracture energy in tension with $G_f = 0.07\ln(1+0.17f_c)$ as shown in [30]. The Young's modulus of the lime mortar in the preliminary model for a compressive strength of 0.6 N/mm^2 linear interpolation yielded $E = 1{,}160$ N/mm^2 with the typical range of 1000-5000 N/mm^2 for $f_c = 0.5-3$ N/mm^2 [22].

The calibrated model parameters, optimized against experimental force-displacement curves, showed significant variations from preliminary values. Brick elements exhibited reduced Young's and shear moduli (-26%), decreased compressive strength (-9.2%), and increased tensile strength (+13.1%).

Table 3. Material properties applied to AEM models

Property	**Experimental (B/M)**	**AEM initial (B/M)**	**AEM calibrated (B/M)**
Density, γ [kg/m^3]	1,923/1,385	1,923/1,385	1,923/1,385
Young's modulus, E [N/mm^2]	-/-	10,800/1,160	7,992/1,765
Compressive strength, f_k [N/mm^2]	10.8/0.6	10.8/0.6	9.81/1.28
Tensile strength, f_t, [N/mm^2]	2.7/0.1*	1.26/0.09	1.42/0.07
Cohesion, c [N/mm^2]	0**	1.76/0.12	0.98/0.10
Friction coefficient, μ [-]	0.66**	0.8/0.6	0.6/0.6
Compressive fracture energy (N/mm)	-/-	16.61/1.81	19.61/2.94
Tensile fracture energy (N/mm)	-/-	0.07/0.007	0.073/2.94
Residual shear strength factor	-/-	0/0	1/0

B/M=Brick/Mortar, * Tensile flexural strength, ** Masonry

DOI: https://doi.org/10.5592/CO/3CroCEE.2025.24

Joint springs representing mortar demonstrated more substantial modifications: increased Young's and shear moduli (+52.2%), doubled compressive strength (0.6 to 1.275 N/mm²), and reduced cohesion (-25.1%). Fracture energies for brick varied slightly (compression: +18.0%, tension: -0.5%), while mortar showed substantial increases (compression: +62.5%, tension: 0.0068 to 2.942 N/mm). RC beams and steel loading plates maintained elastic properties. It should be noted that the calibrated material properties in ELS for the mortar actually represent the stiffnesses of the joint normal and shear springs.

The mechanical response of URM walls exhibits marked sensitivity to boundary conditions. To ensure fidelity with experimental conditions, the analytical model explicitly incorporated the reinforced concrete (RC) beam elements that served dual purposes: the application of vertical pre-compression forces (red arrow in Figure 7) and fully fixed boundary conditions at the wall's base (green arrow in Figure 7). Out-of-plane behaviour was prevented through top RC beam restraint. Loading protocol followed three sequential stages: self-weight (two equal increments), vertical pre-compression (ten equal increments), and cyclic in-plane loading matching experimental patterns, as shown in Figure 1c. Dynamic solution employed 50 time-step intervals between calculations and 20 subdivisions per time step.

4. Results and Discussion

A comparative analysis was conducted between numerical simulations and experimental results for walls URM1 and URM3, examining force-displacement hysteresis and damage progression patterns. Displacement measurements were taken at the load application point on the top beam, with numerical damage characterized through strain patterns and spring corresponding to an ‘open crack’ state in the AEM framework. In AEM and ELS modelling [29], cracks form when spring normal strains exceed zero under specified criteria, allowing simulation of cyclic crack behaviour. Both specimens exhibited shear failure with diagonal and vertical mortar joint cracking and distinctive crack patterns: URM1 initiated damage at diagonal corners at approximately 88 kN during the first loading cycle, before propagation to the centre of the wall, while URM3 showed initiation in the centre at about 84.5 kN with bidirectional expansion. Both walls demonstrated symmetric hysteretic responses, achieving lateral strengths of 197.5 kN and 174.6 kN at displacements of 4.05 mm and 4.4 mm for URM1 and URM3 respectively. At the end of the simulations, comprehensive crack patterns were revealed throughout the wall surfaces, indicating cyclic opening and closing behaviour. The numerical simulation results for URM1, illustrated in Figure 8, demonstrated strong correlation with experimental observations.

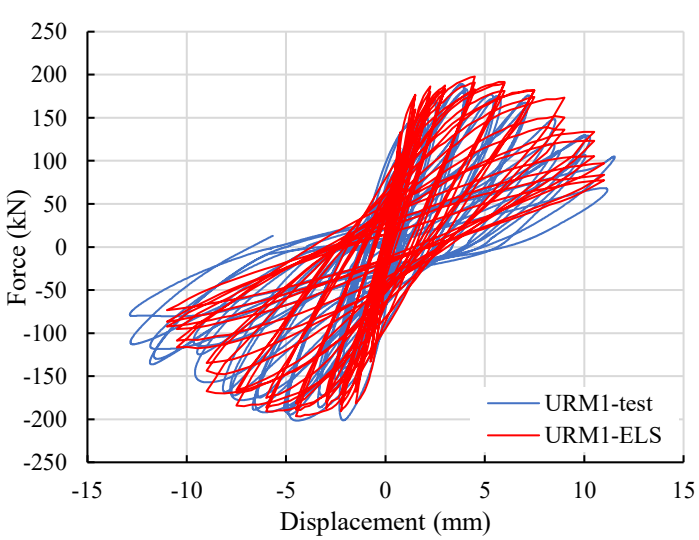

a) Force-displacement hysteresis

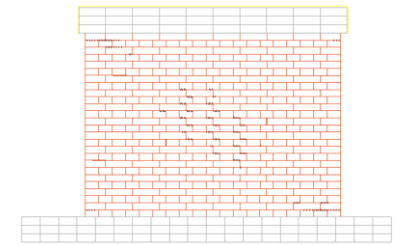

b) Initial progression of damage, open cracks at 1st loading cycle at 119 kN

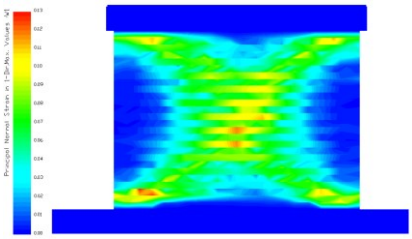

c) Final principal normal strains

Figure 8. Comparison between numerical and experimental response for URM1

DOI: https://doi.org/10.5592/CO/3CroCEE.2025.24

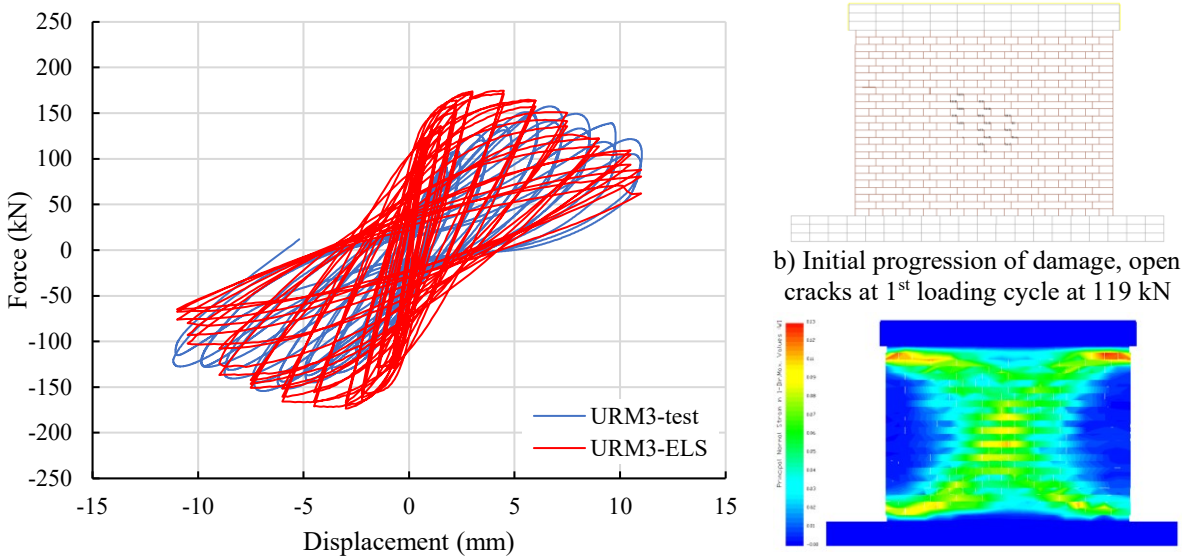

a) Force-displacement hysteresis

b) Initial progression of damage, open cracks at 1st loading cycle at 119 kN

c) Final principal normal strains

Figure 9. Comparison between numerical and experimental response for URM3

The numerical model accurately captured initial and progressive cracking patterns, with lateral strength predictions deviating only 2% from experimental values for URM1 and 10% for URM3. While both models overestimated initial stiffness, they showed good agreement in predicting peak lateral strength displacements (URM1: 4.44 mm experimental vs. 4.05 mm numerical; URM3: 6.67 mm experimental vs. 4.41 mm numerical). URM3's model successfully reproduced the central crack initiation, bidirectional propagation, and diagonal shear failure, though with a slightly different sequence than observed experimentally, as shown in Figure 9.

The overestimated initial stiffness was due to various interrelated factors, including modelling assumptions and experimental testing procedures. The simplified micro-modelling approach is a computationally efficient approach that idealizes certain aspects of masonry behaviour, particularly in the elastic range. Despite carefully calibrating material properties, the model may not fully capture the complex interactions at brick-mortar interfaces, especially during the initial loading phases. Real masonry structures typically contain pre-existing micro-cracks and construction imperfections that influence their initial response, making numerical modelling of such structures quite challenging. Modelling boundary and loading conditions present another significant challenge. The ELS models explicitly incorporated RC beams and attempted to replicate experimental conditions, but certain idealizations were unavoidable. They assumed perfect connection between the masonry wall and RC beams and introduce idealized restraints at the base. However, physical experiments frequently demonstrate unintended flexibility or minor slips at these connections, resulting to a more complex response. The loading apparatus was simplified in the numerical models and assumes perfect vertical and horizontal load applications. During the experiments, the loading control is critical challenge and often some deviations from the idealized conditions are present. From a theoretical perspective, the modelling approach itself introduces certain limitations. The representation of mortar joints through zero-thickness springs, while effective for overall behaviour, may not perfectly capture initial deformation mechanisms. The Concrete Maekawa constitutive model, selected for its robust representation of nonlinear behaviour, might exhibit excessive stiffness in the elastic range. Furthermore, the discrete nature of the AEM could potentially overlook some continuous deformation behaviours characteristic of early loading stages.

Generally, the ELS models successfully captured key physical characteristics of the masonry walls, including maximum forces, displacement limits, and hysteretic behaviour. The simulations accurately represented essential masonry response features such as stiffness degradation and pinching effects near zero force, reflecting progressive damage and cyclic crack behaviour. This strong correlation validates the model's ability to represent complex masonry wall behaviour under seismic loading.

Proceedings of the 3rd Croatian Conference on Earthquake Engineering - 3CroCEE
19–22 March 2025, Split, Croatia

DOI: https://doi.org/10.5592/CO/3CroCEE.2025.24

5. Conclusions and Recommendations

The present study validated the effectiveness of the Applied Element Method modelling unreinforced masonry walls under cyclic in-plane loading. The numerical models demonstrated high accuracy, with lateral strength predictions deviating only 2-10% from experimental values. The simulations successfully captured key behavioural aspects including crack initiation, propagation patterns, stiffness degradation, and pinching effects which are essential features for understanding seismic performance.

While the models effectively predicted overall behaviour, they overestimated initial stiffness. Additionally, computational demands increased significantly with model complexity when replicating the steel loading elements above the top RC beams, potentially limiting applications to large-scale analyses. Nevertheless, the validated approach provides engineers with a reliable tool for seismic assessment, offering calibrated material parameters as references for similar masonry types.

The practical implications of this research are significant for both research and engineering practice, providing engineers with a reliable tool for seismic assessment of masonry structures. The methodology demonstrates particular promise for implementation in performance-based design and assessment frameworks. However, several practical challenges must be addressed for widespread adoption in engineering practice. These include the need for straightforward procedures for material parameter calibration and integration with existing structural analysis software platforms. Additionally, guidelines for verification of AEM models in practice need to be established.

The findings can be cautiously extended to other masonry typologies beyond the lime mortar and clay brick combinations. The fundamental mechanics captured by the AEM approach, including interface behaviour and discrete crack propagation, are applicable to various masonry systems. Yet, the specific material parameters would need recalibration for different combinations such as cement-based mortars, natural stone units, or historical materials. The methodology's ability to capture brittle failure mechanisms suggests particular applicability to heritage structures built with traditional materials.

Future research should address combined in-plane and out-of-plane loading effects, development of more computationally efficient methods. Additional validation through full-scale dynamic testing, different strengthening techniques applied to existing masonry assemblages and incorporation of aging effects would further enhance the method's applicability to historical structures. The study's findings contribute significantly to masonry modelling knowledge while highlighting areas requiring continued development to expand AEM's practical applications in structural engineering.

Acknowledgements

In this paper, I would like to thank Professor Elena Dumova-Jovanoska, Ss. Cyril and Methodius University in Skopje, Faculty of Civil Engineering Skopje, for the encouragement she gave me during my work as a doctoral student, more than twelve years ago that continues to be relevant even in this research work.

The author gratefully acknowledges Mr. Ayman Elfouly, P.E., Senior Consulting Engineer at Applied Science International, LLC (ASI) for his invaluable support and technical expertise in the ELS software analysis, which significantly enhanced the quality of this research.

References

[1] Roca, P., Cervera, M., Gariup, G., Pela, L. (2010): Structural analysis of masonry historical constructions. Classical and advanced approaches, *Archives of Computational Methods in Engineering*, **17** (3), 299–325, https://doi.org/10.1007/s11831-010-9046-1.

[2] Magenes, G., Calvi, G.M. (1997): In-plane seismic response of brick masonry walls, *Earthquake Engineering & Structural Dynamics*, **26** (11), 1091–1112, https://doi.org/10.1002/(SICI)1096-9845(199711)26:11.

[3] Asteris, P.G., Sarhosis, V., Mohebkhah, A., Plevris, V. (2015): (2015), Numerical modeling of historic masonry structures, in *Handbook of Research on Seismic Assessment and Rehabilitation of Historic Structures, IGI Global*, 213–256. https://doi.org/10.4018/978-1-4666-8286-3.

DOI: https://doi.org/10.5592/CO/3CroCEE.2025.24

[4] Giordano, A., Mele, E., Luca, A. (2002): Modelling of historical masonry structures: comparison of different approaches through a case study, *Engineering Structures*, **24** (8), 1057–1069, https://doi.org/10.1016/S0141-0296(02)00033-0.

[5] Theodossopoulos, D., Sinha, B. (2013): A review of analytical methods in the current design processes and assessment of performance of masonry structures, *Construction and Building Materials*, **41**, 990–1001, https://doi.org/10.1016/j.conbuildmat.2012.07.095.

[6] Meguro, K., Tagel-Din, H. (2000): Applied Element Method for structural analysis: Theory and application for linear materials, *Structural Engineering/Earthquake Engineering*, **17** (1), 31–45.

[7] Malomo, D., Pinho, R., Penna, A. (2018): Using the Applied Element Method to simulate the dynamic response of full-scale URM houses tested to collapse or near-collapse conditions, in *Proceedings of 16th European Conference on Earthquake Engineering*, Thessaloniki, Greece.

[8] Malomo, D., Pinho, R., Penna, A. (2018): Using the applied element method for modelling calcium silicate brick masonry subjected to in-plane cyclic loading, *Earthquake Engineering & Structural Dynamics*, **47** (7), 1610–1630, https://doi.org/10.1002/eqe.3032.

[9] Mayorca, P., Meguro, K. (2003): Modeling Masonry Structures using the Applied Element Method, *Seisan-Kenkyu*, **55** (6), 123–126.

[10] Christy, D.L., Pillai, T.M.M., Nagarajan, P. (2018): Analysis of Brick Masonry Wall using Applied Element Method, *IOP Conference Series: Materials Science and Engineering*, **330**, 012128, https://doi.org/10.1088/1757-899X/330/1/012128.

[11] Eraky, A., Mustafa, S.A., Badawy, M. (2021): Structural Analysis using Applied Element Method: A Review, *The Egyptian International Journal of Engineering Sciences and Technology*, **34** (1), 16–27, https://doi.org/10.21608/eijest.2021.56786.1043.

[12] Gohel, V., Patel, P.V., Joshi, D. (2013): Analysis of Frame using Applied Element Method (AEM), *Procedia Engineering*, **51**, 176–183, https://doi.org/10.1016/j.proeng.2013.01.026.

[13] Khattak, N., Derakhshan, H., Thambiratnam, D.P., Malomo, D., Perera, N.J. (2023): Modelling the in-plane out-of-plane interaction of brick and stone masonry structures using Applied Element Method, *Journal of Building Engineering*, **76**, 107175, https://doi.org/10.1016/j.jobe.2023.107175.

[14] Adhikari, R.K., Parammal Vatteri, A., D'Ayala, D. (2023): Seismic Performance Assessment of Low-Rise Unreinforcedand Confined Brick Masonry School Buildings Using the Applied Element Method, *Buildings*, **13**, 159, https://doi.org/10.3390/buildings13010159.

[15] Karbassi, A., Nollet, M.-J. (2013): Performance-Based Seismic Vulnerability Evaluation of Masonry Buildings Using Applied Element Method in a Nonlinear Dynamic-Based Analytical Procedure, *Earthquake Spectra*, **29** (2), 399–426, https://doi.org/10.1193/1.4000148.

[16] Pandey, B., Meguro, K. (2004): Simulation Of Brick Masonry Wall Behavior Under Inplane Lateral Loading Using Applied Element Method, in *13th World Conference on Earthquake Engineering*, Vancouver, B.C., Canada, August.

[17] Sharma, S., Marasca, A., Ponte, M., Bento, R. (2022): Modelling the in-plane cyclic behaviour of typical Portuguese rubble stone masonry using the applied element method, *Structures*, **46**, 1224–1242, https://doi.org/10.1016/j.istruc.2022.10.107.

[18] Canditone, C., Parisi, F. (2024): Numerical simulation of soft stone masonry under simple compression using the Applied Element Method, in *18th World Conference on Earthquake Engineering*, Milan, Italy.

[19] Churilov, S. (2012): *Experimental and analytical research of strengthened masonry*. PhD dissertation, Ss. Cyril and Methodius University, Faculty of Civil Engineering-Skopje.

[20] Churilov, S., Dumova-Jovanoska, E. (2013): In-plane shear behaviour of unreinforced and jacketed brick masonry walls, *Soil Dynamics and Earthquake Engineering*, **50**, 85–105, https://doi.org/10.1016/j.soildyn.2013.03.006.

[21] Binda, L., Fontana, A., Frigerio, G. (1988): Mechanical behaviour of brick masonries derived from unit and mortar characteristics, in *8th International Brick and Block Masonry Conference*, Dublin, Ireland, 205–216.

DOI: https://doi.org/10.5592/CO/3CroCEE.2025.24

[22] Kržan, M., Gostič, S., Cattari, S., Bosiljkov, V. (2015): Acquiring reference parameters of masonry for the structural performance analysis of historical buildings, *Bulletin of Earthquake Engineering*, **13**, 203–236, https://doi.org/10.1007/s10518-014-9686-x.

[23] Kaushik, H.B., Durgesh, R.C., Sudhir, J.K. (2007): Stress- strain characteristics of clay brick masonry under uniaxial compression, *Journal of Materials in Civil Engineering*, **19** (9), 728–739, https://doi.org/10.1061/(ASCE)0899-1561(2007)19:9(728).

[24] Tomaževič, M. (2009): Shear resistance of masonry walls and Eurocode 6: shear versus tensile strength of masonry, *Materials and Structures*, **42**, 889-907,, https://doi.org/10.1617/s11527-008-9430-6.

[25] Morandi, P., Magenes, G., Albanesi, L. (2013): Prove Sperimentali per la Valutazione della Risposta Sismica nel Piano di Pareti Murarie in Blocchi di Laterizio a Setti Sottili, in *Proceedings of the XV Convegno Nazionale ANIDIS - "L'ingegneria sismica Italiana"*, Padua, Italy.

[26] Salmanpour, A.H., Mojsilović, N., Schwartz, J. (2015): Displacement capacity of contemporary unreinforced masonry walls: An experimental study, *Engineering Structures*, **80**, 1-16,, https://doi.org/10.1016/j.engstruct.2015.01.052.

[27] Morandi, P., Albanesi, L., Magenes, G. (2014): URM walls with thin shell/web clay units and unfilled head-joints: Cyclic in-plane tests, in *Proceedings of the 2nd European Conference on Earthquake Engineering and Seismology*, Istanbul, Turkey.

[28] Hrasnica, M., Biberkić, F., Medić, S. (2018): Experimental testing of solid brick masonry walls, *Key Engineering Materials*, **747**, 694–701, https://doi.org/10.4028/www.scientific.net/KEM.747.694.

[29] Applied Science International, LLC. (2024): *Extreme loading for Structures, Theoretical Manual, version 01*.

[30] Lourenço, P.B., Gaetani, A. (2022): *Finite Element Analysis for Building Assessment - Advanced Use and Practical Recommendations*, 1st ed. New York, USA: Routledge, Taylor & Francis Group. https://doi.org/10.1201/9780429341564.

[31] Christy, C.F., Tensing, D., Shanthi, R.M. (2012): In-plane shear behaviour of Brick Masonry - A Literature Review on experimental study, *International Journal of Civil and Structural Engineering*, **2** (4), 1144–1152.

[32] Kumar, K.H., Tripathi, R.K. (2024): Damage assessment of infilled frame structures using applied element method, *Bulletin of Earthquake Engineering*, **22**, 1387–1423, https://doi.org/10.1007/s10518-023-01824-6.

[33] Malomo, D., Pinho, R., Penna, A. (2020): Applied element modelling of the dynamic response of a full-scale clay brick masonry building specimen with flexible diaphragms, *International Journal of Architectural Heritage*, **14** (10), 1484–1501, https://doi.org/10.1080/15583058.2019.1616004.

[34] Maekawa, K., Okamura, H. (1983): Deformational Behavior and Constitutive Equation of Concrete using the Elasto-Plastic and Fracture Model, *Journal of the Faculty of Engineering*, **37** (2), 253–328.

[35] Okamura, H., Maekawa, K. (1991): *Nonlinear analysis and constitutive models of reinforced concrete*. Giho-do Press, Tokyo, Japan.

[36] El-Kashif, K.F., Maekawa, K. (2004): Time-dependent nonlinearity of compression softening in concrete, *Journal of Advanced Concrete Technology*, **2** (2), 233–247, https://doi.org/10.3151/jact.2.233.

[37] Lourenço, P.B. (1996): *Computational Strategies for Masonry Structures*. PhD dissertation, Delft University of Technology, Delft, Netherlands.